Journal of Sound and Vibration (2002) **256**(4), 755–771
doi:10.1006/jsvi.5019, available online at http://www.idealibrary.com on IDEAL®

AN ANALYTICAL AND NUMERICAL STUDY OF A MODIFIED VAN DER POL OSCILLATOR

E. J. Doedel

Computer Science Department, Concordia University, Montreal, Canada

AND

E. Freire, E. Gamero and A. J. Rodríguez-Luis

Department of Applied Mathematics II, Escuela Superior de Ingenieros, University of Sevilla, 41092 *Sevilla, Spain. E-mail: alejan@matina.us.es*

(*Received* 10 *August* 2001, *and in final form* 11 *January* 2002)

A three-dimensional system of differential equations that models an electronic oscillator is considered. The equations allow a variety of periodic orbits that originate from a degenerate Hopf bifurcation, which is analytically studied. Numerical results are presented that show the existence of saddle-node cusps of periodic orbits, as well as period-doubling bifurcations, that result in the coexistence of multiple "canard" orbits if one of the parameters is small. The presence of chaotic attractors is also detected.

1. INTRODUCTION

Electronic devices have played an important role in the theory of dynamical systems. They have been a source of both theoretical and numerical development, and they may be the simplest and cheapest physical devices where complex dynamical behaviour can be determined analytically, numerically and experimentally.

A van der Pol system provides a first example of an oscillator with non-linear damping that typically possesses limit cycles. The original equation described by van der Pol [1] models an electrical circuit with a triode valve. A modern version of such a circuit appears in Figure 1(a) when $a = 0$ (no battery), where $f(x)$ represents the non-linear characteristic of a negative conductance. It is well known that, for small values of the capacity C_0, this system has a stable limit cycle in the form of a relaxation oscillation (see reference [2]).

If a battery is added (see Figure 1(a) the system may exhibit *canard* orbits. The canard phenomenon, typical in singularly perturbed systems, was first found, precisely, in the van der Pol modified equation that takes into account the presence of the battery. (The name *canard*, duck in French, was suggested by the phase-plane appearance of these periodic orbits.) Their existence was shown by non-standard analysis techniques (see references [3–6]). It is also possible to obtain some information about canard explosion without the use of non-standard analysis techniques [7–10]. The canard phenomenon appears as a bridge linking the local dynamics, represented by the small-amplitude limit cycles born in the Hopf bifurcation, and the global dynamics corresponding to relaxation oscillations.

More recently, several works have dealt with canards in tridimensional systems (see references [11, 12]).

0022-460X/02/$35.00

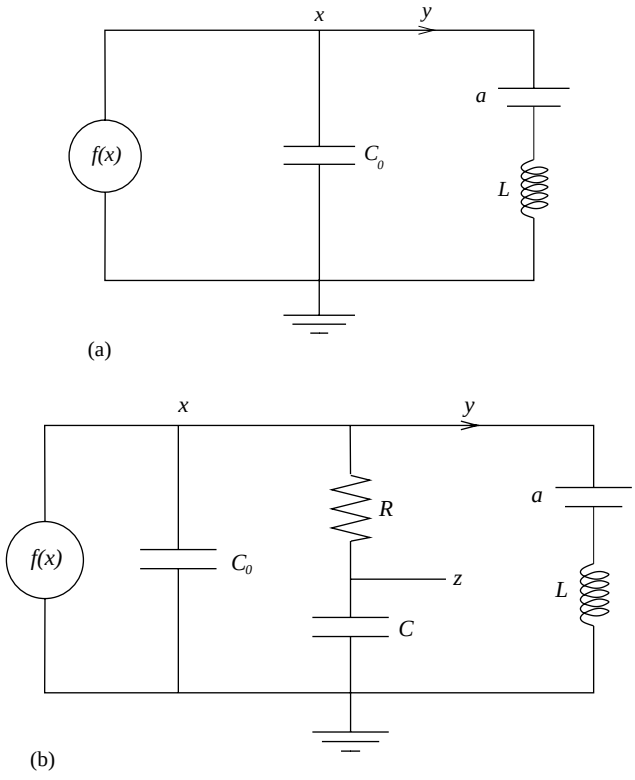

Figure 1. Circuit schemes: (a) modern version of the van der Pol circuit with a battery added; (b) three-dimensional modified van der Pol circuit by including a linear RC parallel branch.

On the other hand, several ways to obtain a three-state electronic circuit from a van der Pol configuration have been proposed in the last decades (see references [13–17]). A review of these different configurations can be found in Freire *et al.* [18]. Note that all of them may have more than one equilibrium and then, local bifurcations of equilibria such as fold, pitchfork (in the case of symmetry), Takens–Bogdanov, Hopf–pitchfork, etc. will appear.

In the present paper, a different configuration is proposed in order to obtain a system with only one equilibrium. This is achieved introducing a linear RC parallel branch (see Figure 1(b)).

The analysis focuses on periodic oscillations in this simple autonomous electronic system. The system contains a parameter that will allow the generation of relaxation oscillations and periodic orbits of canard type when it is small.

The approach shown in this work is based on an analytical study of limit cycles near a Hopf bifurcation, using centre manifold reduction and normal form computation (see, for instance, reference [19]). Specifically the geometrical theory of Fenichel [20] (see also reference [21]) is used. In this framework, inside the geometrical theory of dynamical systems, the results obtained are analogous to those provided by the boundary layer theory.

This paper is organized as follows. In section 2, the system of differential equations that models the electronic oscillator is derived. To analyze the Hopf bifurcation where the

periodic oscillations are born, a reduced system is first considered in section 2.1. The results obtained are helpful in the analysis of the full system, carried out in section 2.2. In section 3, some numerical results are presented. They show the presence of folds, cusps, and period-doubling bifurcations along branches of periodic solutions, resulting in the coexistence of multiple canard orbits if the corresponding parameter is small enough. Chaotic régime has also been found. Finally, some conclusions and remarks appear in section 4.

2. ANALYSIS OF THE MODEL

The electronic circuit considered is shown in Figure 1(b). As stated above, it is obtained from the van der Pol circuit with a battery, sketched in Figure 1(a), by adding a linear RC parallel branch. This electronic device has two capacitors C_0 and C, an inductance L, a resistor R, a DC source that provides a voltage a, and a non-linear negative conductance whose voltage–current characteristic $f(x)$ is approximated by the cubic polynomial

$$f(x) = -a_1 x + a_3 x^3, \quad a_1, a_3 > 0.$$

Application of Kirchhoff's laws gives the equations that govern the dynamics of the oscillator, namely,

$$C_0 \dot{x} = -f(x) + \frac{(z-x)}{R} - y, \qquad L\dot{y} = x - a, \qquad C\dot{z} = -\frac{(z-x)}{R},$$

where x denotes the voltage across capacitor C_0, y the inductance current and z the voltage across capacitor C.

Rescaling the state and time variables

$$x = V_0 \bar{x}, \qquad y = \frac{V_0}{\omega L}\bar{y}, \qquad z = V_0 \bar{z}, \qquad \tau = \omega t,$$

where

$$\omega = \frac{1}{\sqrt{LC}}, \qquad V_0 = \sqrt{\frac{a_1}{3a_3}},$$

defining new parameters

$$\varepsilon = \frac{C_0}{C}, \qquad \bar{a} = \frac{a}{V_0}, \qquad \alpha = \frac{a_1}{\omega C}, \qquad \bar{R} = R\omega C,$$

and omitting the bars, the following system is obtained:

$$\varepsilon \dot{x} = -g(x) + \frac{(z-x)}{R} - y, \quad \dot{y} = x - a, \qquad \dot{z} = -\frac{(z-x)}{R}, \tag{1}$$

where

$$g(x) = \alpha\left(\frac{x^3}{3} - x\right).$$

Note that the equations governing the circuit of Figure 1(a) are obtained from equation (1) in the limit $R \to \infty$.

For fixed a this system has a single equilibrium point, namely $(x_0, y_0, z_0) = (a, -g(a), a)$ with Jacobian

$$J = \begin{pmatrix} \frac{\alpha}{\varepsilon}(1-a^2) - \frac{1}{\varepsilon R} & -\frac{1}{\varepsilon} & \frac{1}{\varepsilon R} \\ 1 & 0 & 0 \\ \frac{1}{R} & 0 & -\frac{1}{R} \end{pmatrix}.$$

The characteristic polynomial of J is $P(\lambda) = \lambda^3 + A_1\lambda^2 + A_2\lambda + A_3$, with

$$A_1 = -\frac{1}{\varepsilon}\left[\alpha(1-a^2) - \frac{1}{R}\right] + \frac{1}{R}, \qquad A_2 = \frac{1}{\varepsilon}\left[1 - \frac{\alpha}{R}(1-a^2)\right], \qquad A_3 = \frac{1}{\varepsilon R}.$$

A necessary condition for a Hopf bifurcation can be obtained by imposing the existence of an imaginary complex pair of eigenvalues, $\pm i\omega$, and a real one, $\lambda_R \neq 0$, in

$$P(\lambda) = (\lambda^2 + \omega^2)(\lambda - \lambda_R) = \lambda^3 - \lambda_R\lambda^2 + \omega^2\lambda - \omega^2\lambda_R.$$

Then, the necessary condition is $A_1A_2 = A_3$ with $A_2 > 0$, $A_1 \neq 0$. In the present case, this leads to

$$\varepsilon s = (1 - Rs)(R - s), \quad R > s,$$

where $s = \alpha(1 - a^2)$. This expression defines the Hopf curve

$$a^2 = 1 - \frac{1 + R^2 + \varepsilon - \sqrt{(1 + R^2 + \varepsilon)^2 - 4R^2}}{2\alpha R} \tag{2}$$

in the R–a parameter plane. It is easy to check that, in the above formula,

$$(1 + R^2 + \varepsilon)^2 - 4R^2 > 0 \quad \text{for all} \quad R, \varepsilon > 0.$$

2.1. ANALYSIS OF THE REDUCED SYSTEM

As it will be shown, an important feature of the above system is that it exhibits three-dimensional canard periodic orbits if ε is small enough. However, before analyzing their associated Hopf bifurcations, the reduced system obtained setting $\varepsilon = 0$ in equation (1) is considered, namely,

$$\dot{y} = x - a, \qquad \dot{z} = \frac{(x - z)}{R}, \qquad y = -g(x) + \frac{(z - x)}{R}. \tag{3}$$

Knowledge of the dynamics of this reduced system will be useful in the understanding of the bifurcation behaviour of the full system. For the existence of canard orbits, the slow manifold must have a fold, i.e., the coefficients of x and x^3 in the last equation (3) must have opposite signs. This is the case when $R > 1/\alpha$. The two possible situations are sketched in Figure 2.

The equilibrium state of equation (3) is the same as that of equation (1), namely, $(a, -g(a), a)$. Using the algebraic equation (3) for the computation of the partial derivatives of x with respect to y and z, the Jacobian at the equilibrium of the reduced (x, y)-system is

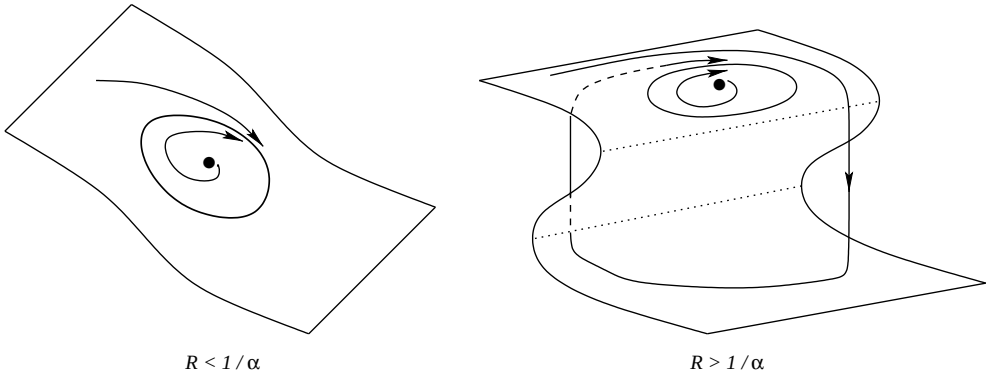

Figure 2. Qualitative form of the slow manifold of system (1). Note that it has no fold if $R < 1/\alpha$. Some trajectories close to a periodic orbit emerged from a Hopf bifurcation are also sketched in the case of small ε.

given by

$$\mathbf{A} = \begin{pmatrix} \dfrac{-R}{1-Rs} & \dfrac{1}{1-Rs} \\ \dfrac{-1}{1-Rs} & \dfrac{s}{1-Rs} \end{pmatrix},$$

where $s = \alpha(1 - a^2)$. The Hopf condition is $R = s,\ R < 1$, which also corresponds to the limiting curve in equation (2) when $\varepsilon \to 0$.

It is of interest to determine when the equilibrium is located at the relative minimum or relative maximum of the cubic. For the appearance of canard orbits, the equilibrium has to be close to this position, so that the orbit can reach and stay on the unstable part of the slow manifold. An easy computation shows that the equilibrium is at this location when $Rs = 1$. This locus will be called *barrier*. Since the Hopf condition $R < 1$ results from

$$\det \mathbf{A} = \frac{1}{(1 - Rs)} > 0,$$

the Hopf curve in the reduced system (labelled *HR* in Figure 3), exists until it reaches the barrier *BA*. This intersection exists only if $\alpha \geqslant 1$ and occurs at $R = 1$ (see Figure 3(c)).

To analyze the Hopf bifurcation, a is taken as the bifurcation parameter. At the critical value $a = a_c$, where $a_c^2 = (1 - R/\alpha)$, the equilibrium point has eigenvalues $\pm\, \omega_0 \mathrm{i}$, with $\omega_0^2 = 1/(1 - R^2)$. Consequently, the existence of the Hopf bifurcation requires both $R < 1$ and $R < \alpha$. It is easy to check the transversality condition, that is, that the pair of conjugate complex eigenvalues, λ and $\bar{\lambda}$, crosses the imaginary axis with non-zero velocity:

$$Re\left[\left.\frac{\mathrm{d}\lambda}{\mathrm{d}a}\right|_{a=a_c}\right] = \frac{-a_c\alpha}{(1 - R^2)} \neq 0, \quad \text{whenever } a_c,\ \alpha \neq 0. \tag{4}$$

To study the stability of the bifurcation, its normal form is computed. Fixing the parameter at its critical value $a = a_c$, translating the equilibrium point to the origin

$$\bar{y} = y - \alpha a_c\left(1 - \frac{a_c^2}{3}\right), \qquad \bar{z} = z - a_c, \qquad \bar{x} = x - a_c, \tag{5}$$

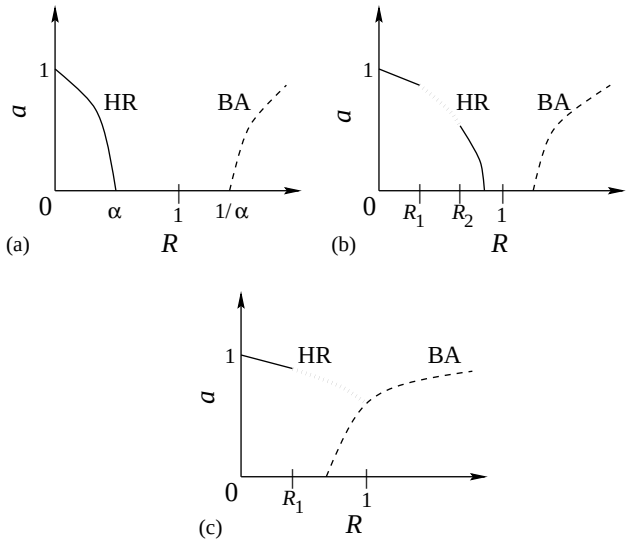

Figure 3. Hopf bifurcation curve *HR* (solid/dotted indicates supercritical/subcritical) of the reduced system: (a) $\alpha < \sqrt{3}/2$; (b) $\sqrt{3}/2 < \alpha < 1$; (c) $\alpha > 1$. The barrier *BA*, that starts at point $(1/\alpha, 0)$, is also drawn.

and changing variables

$$\bar{y} = y^*, \qquad \bar{z} = Ry^* - \omega_0(1 - R^2)z^*,$$

system (3) can be written in the standard form:

$$\begin{pmatrix} \dot{y}^* \\ \dot{z}^* \end{pmatrix} = \begin{pmatrix} 0 & -\omega_0 \\ \omega_0 & 0 \end{pmatrix} \begin{pmatrix} y^* \\ z^* \end{pmatrix} + \begin{pmatrix} \phi(z^*) + \omega_0 z^* \\ \left[\dfrac{-\phi(z^*)}{\omega_0} - z \right] \dfrac{1}{R} \end{pmatrix}, \tag{6}$$

where $\phi(z^*)$ represents the function $\bar{x} = \phi(z^*)$ defined implicitly in a neighbourhood of the origin by

$$\alpha\bar{x}\left(1 - a_c^2 - a_c\bar{x} - \frac{\bar{x}^2}{3}\right) - \frac{\omega_0(1 - R^2)}{R} z^* - \frac{\bar{x}}{R} = 0. \tag{7}$$

This equation follows from equation (3) and from the above change of variables. The normal form for equation (6), in polar co-ordinates $y^* = \rho\cos\theta$, $z^* = \rho\sin\theta$, is (see, for instance, reference [19])

$$\dot{\rho} = a_3\rho^3 + a_5\rho^5 + \cdots, \qquad \dot{\theta} = \omega_0 + \cdots. \tag{8}$$

To get the normal form coefficients a_3, a_5 (which, as will be noted later, characterize the stability of the Hopf bifurcation) it is sufficient to compute derivatives up to fifth order of $\phi(z^*)$ at $z^* = 0$. These are obtained from equation (7):

$$\phi'(0) = -\omega_0, \qquad \phi''(0) = -2a_c\alpha R\omega_0^4, \qquad \phi'''(0) = (2\alpha - 12a_c^2\alpha^2 R\omega_0^2)\omega_0^5 R$$

and

$$\phi^{(\mathrm{iv})}(0) = \frac{40a_c R^2\omega_0^4\alpha^2(R^2 + 3a_c^2 R\alpha - 1)}{(R^2 - 1)^3},$$

$$\phi^{(\mathrm{v})}(0) = \frac{40R^2\omega_0^5\alpha^2(-R^4 - 21a_c^2\alpha R^3 - 42a_c^4\alpha^2 R^2 + 21a_c^2\alpha R + 2R^2 - 1)}{(R^2 - 1)^4}.$$

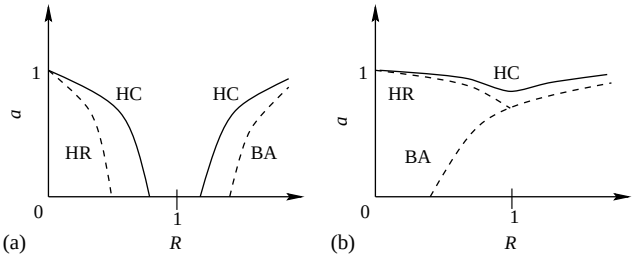

Figure 4. Hopf bifurcation curve *HC* for the full system: (a) with splitting ($\alpha < 1$); (b) without splitting ($\alpha > 1$). The Hopf bifurcation curve for the reduced system *HR* and the barrier *BA* are also sketched.

By means of a recursive symbolic algorithm developed by Freire *et al.* [22], the following expression for the first radial coefficient is obtained:

$$a_3 = \frac{-\omega_0^4 \alpha}{8}(1 - 4a_c^2 \alpha R \omega_0^2).$$

When $a_3 \neq 0$, the presence of a non-degenerate Hopf bifurcation can be assured. For a_3 positive a subcritical Hopf bifurcation takes place, that is, an unstable equilibrium point becomes stable and a repelling limit cycle emerges. On the other hand, for a_3 negative the Hopf bifurcation is supercritical, namely the equilibrium changes from stable to unstable and the emerged periodic orbit is attracting (see, for instance, references [19, 23]). Now $a_3 = 0$ occurs if $3R^2 - 4\alpha R + 1 = 0$. Then a_3 vanishes if $\alpha \geqslant \sqrt{3}/2$. Depending on the value of α, the following situations can occur (see Figure 3):

$\alpha < \sqrt{3}/2$: the Hopf bifurcation *HR* is supercritical for all $R \in (0, \alpha)$.

$\alpha = \sqrt{3}/2$: the Hopf bifurcation is always supercritical, except for $R = \sqrt{3}/3$ where $a_3 = 0$.

$\sqrt{3}/2 < \alpha < 1$: there are two values, R_1 and R_2, with $0 < R_1 < \sqrt{3}/3 < R_2 < 1$, such that the bifurcation is supercritical for $R \in (0, R_1) \cup (R_2, \alpha)$ and subcritical when $R \in (R_1, R_2)$.

$\alpha = 1$: the bifurcation is supercritical for $R \in (0, \frac{1}{3})$ and subcritical for $R \in (\frac{1}{3}, 1)$.

$\alpha > 1$: there is a value $0 < R_1 < \frac{1}{3}$ such that the Hopf bifurcation is supercritical for $R \in (0, R_1)$ and subcritical for $R \in (R_1, 1)$. As α increases, the supercritical region shrinks because $\lim_{\alpha \to \infty} R_1(\alpha) = 0$.

For the parameter values where the first coefficient of the Hopf bifurcation vanishes, the following expression for the second coefficient is also obtained:

$$a_5 = -\frac{720R^6 + 489R^4 + 86R^2 + 1}{12\,288R^3(R^2 - 1)^4}.$$

This coefficient is always negative, so that no higher order degeneracies appear.

2.2. ANALYSIS OF THE HOPF BIFURCATION FOR THE FULL SYSTEM

Given the results for the reduced system, the Hopf bifurcation in the full system with $\varepsilon \neq 0$ is now analyzed (see references [20, 21]). The Hopf curve, given in equation (2), is labelled as *HC* in Figure 4. This curve lies above the Hopf curve of the reduced system *HR* for $R < 1$ and above the barrier *BA* for $R > 1$. Furthermore, these curves approach each other as $\varepsilon \to 0$. Thus, for $\alpha < 1$ and ε small enough, the Hopf curve may split, that is, there may exist values of R for which expression (2) has no solution. Fixing one of the parameters α, R and ε, for example ε, one can check that the splitting of the curve ($a = 0$) occurs for

uniquely determined values of the other two parameters. Specifically, one finds that $\alpha = \sqrt{1+\varepsilon} - \sqrt{\varepsilon}$, $R = \sqrt{1+\varepsilon}$.

For the equilibrium, the following results hold. If $a > 0$, then it is stable above the Hopf curve and it is a saddle below the Hopf curve. If $a < 0$, then it is a saddle above the Hopf curve and it is stable below the Hopf curve. It is enough to focus on the case $a > 0$, as the system is invariant to the change $(x, y, z, a) \to (-x, -y, -z, -a)$.

The analysis of the Hopf bifurcation is carried out in the following. As in section 2.1, a is taken as bifurcation parameter. Now the Hopf bifurcation occurs at the critical value $a = a_c$ given in equation (2). For this critical value, the equilibrium point has eigenvalues $\pm \omega_0 \mathrm{i}$ and λ_0 given by

$$\omega_0^2 = \frac{R - \alpha(1 - a_c^2)}{\varepsilon R}, \qquad \lambda_0 = -\frac{1}{(R - s_0)},$$

where $s_0 = \alpha(1 - a_c^2)$.

The transversality condition holds because

$$Re\left[\left.\frac{\mathrm{d}\lambda}{\mathrm{d}a}\right|_{a=a_c}\right] = -\frac{a_c \alpha \omega_0^2 (1 + \varepsilon R^2 \omega_0^4)}{(1 + \varepsilon^2 R^2 \omega_0^6)} \neq 0 \quad \text{for } a_c, \alpha \neq 0. \tag{9}$$

Note that, for $\varepsilon = 0$, the transversality conditions of the reduced system (4) and of the full system (9) agree.

To determine the stability of the Hopf bifurcation, the equilibrium point is translated to the origin, using the same change of variables as for the reduced system, namely equation (5). This gives the system

$$\varepsilon \dot{\bar{x}} = s\bar{x} + \frac{(\bar{z} - \bar{x})}{R} - \bar{y} - \alpha \bar{x}^2 \left(a + \frac{\bar{x}}{3}\right), \qquad \dot{\bar{y}} = \bar{x}, \qquad \dot{\bar{z}} = -\frac{(\bar{z} - \bar{x})}{R}.$$

With the change of variables

$$\begin{pmatrix} \bar{x} \\ \bar{y} \\ \bar{z} \end{pmatrix} = \begin{pmatrix} 1 & 0 & \lambda_0 \\ 0 & \dfrac{1}{\omega_0} & 1 \\ \dfrac{s_0}{\omega_0^2 R} & \dfrac{s_0}{\omega_0} & \dfrac{1}{s_0} \end{pmatrix} \begin{pmatrix} x^* \\ y^* \\ z^* \end{pmatrix},$$

the matrix is put in Jordan form

$$\begin{pmatrix} \dot{x}^* \\ \dot{y}^* \\ \dot{z}^* \end{pmatrix} = \begin{pmatrix} 0 & -\omega_0 & 0 \\ \omega_0 & 0 & 0 \\ 0 & 0 & \lambda_0 \end{pmatrix} \begin{pmatrix} x^* \\ y^* \\ z^* \end{pmatrix} + \xi(x^*, z^*) \begin{pmatrix} \lambda_1 \\ \lambda_2 \\ \lambda_3 \end{pmatrix},$$

where

$$\xi(x^*, z^*) = -\frac{\alpha \lambda_0 s_0}{K_1} \left(a_c + \frac{\bar{x}}{3}\right) \bar{x}^2, \qquad \bar{x} = x^* + \lambda_0 z^*, \qquad K_1 = \frac{1}{s_0} - s_0 - \frac{\lambda_0 s_0}{\omega_0^2 R},$$

$$\lambda_1 = \frac{s_0^2 - 1}{s_0(1 - R s_0)}, \qquad \lambda_2 = -\omega_0, \lambda_3 = 1.$$

Now the centre manifold is computed, using a recursive procedure described in Freire *et al.* [24]. Dropping the asterisks, it is given by

$$z = \alpha_1 x^2 + \alpha_2 y^2 + \alpha_{12} xy + \cdots,$$

where

$$\alpha_1 = -\frac{\lambda_0^2 + 2\omega_0^2}{\lambda_0(\lambda_0^2 + 4\omega_0^2)} a_c K_2, \qquad \alpha_2 = -\frac{2\omega_0^2}{\lambda_0(\lambda_0^2 + 4\omega_0^2)} a_c K_2, \qquad \alpha_{12} = \frac{2\omega_0}{(\lambda_0^2 + 4\omega_0^2)} a_c K_2,$$

with $K_2 = -(\lambda_0 s_0 \alpha)/K_1$.

The reduced system on the centre manifold, up to third order, is

$$\begin{pmatrix} \dot{x} \\ \dot{y} \end{pmatrix} = \begin{pmatrix} 0 & -\omega_0 \\ \omega_0 & 0 \end{pmatrix} \begin{pmatrix} x \\ y \end{pmatrix} + K_2 \Psi(x, y) \begin{pmatrix} \lambda_1 \\ \lambda_2 \end{pmatrix},$$

where

$$\Psi(x, y) = a_c x^2 + (\tfrac{1}{3} + 2a_c\lambda_0\alpha_1)x^3 + 2a_c\lambda_0\alpha_2 xy^2 + 2a_c\lambda_0\alpha_{12} x^2 y.$$

Next, a near-identity transformation brings this last system into the normal form (8). Now the expression for the third order normal form coefficient is

$$a_3 = -\frac{\alpha s_0}{8} \frac{\Omega(R, s_0)}{(1 - Rs_0)[R(1 - Rs_0) + s_0(R - s_0)^2][R(1 - Rs_0) + 4s_0(R - s_0)^2]},$$

where the denominator is always positive and

$$\Omega(R, s_0) = (1 - s_0)^2[R(1 - Rs_0) + 4s_0(R - s_0)^2] - 4(\alpha - s_0)s_0^2[(1 - s_0^2) + s_0(R - s_0)].$$

First, it is checked that the vanishing of a_3 in the full system leads to the same equation for $\varepsilon = 0$ as the vanishing of a_3 in the reduced system. It is sufficient to set $R = s_0$ (which implies $\varepsilon = 0$) to get again the relation $3R^2 - 4\alpha R + 1 = 0$. Therefore, for values of ε close to zero, the results for the reduced system, which are valid for $R < 1$, can be used to find parameter values where a_3 vanishes in the full system.

As in section 2.1, in order to look for canard orbits, it is useful to know if the normal form coefficient a_3 vanishes when the equilibrium is located on the barrier. (Here it is also assumed that $R > 1$.) Thus, setting $Rs_0 = 1$, the equation $\Omega(R, s_0) = 0$ is equivalent to

$$(R^2 - 1)^2 - 2(\alpha R - 1) = 0.$$

It is not difficult to check that the above equation has no solution if $\alpha < \alpha_0$, and two solutions if $\alpha_0 < \alpha < 1$, where $\alpha_0 \approx 0{\cdot}91269$.

With this information, it is concluded that for small ε (see references [20, 21]) there are zones in the ε–α parameter plane where the Hopf curve (in the R–a plane) has up to four degenerate points: for increasing R, the bifurcation is initially supercritical and becomes subcritical, again supercritical, subcritical and finally supercritical. Numerical results confirm these observations. For example, for $\alpha = 0{\cdot}91$ and $\varepsilon = 0{\cdot}021$ (a point in zone III of Figure 5) four degenerate points can be numerically detected on the Hopf curve, in the (R, a) parameter plane. They are placed approximately at (0·44239, 0·72535), (0·95483, 0·24301), (1·00830, 0·22108) and (1·17499, 0·32947).

However, as ε increases, the numerical analysis indicates that some of the degenerate points coalesce. Looking at the ε–α plane in the neighbourhood of the point $(\varepsilon = 0, \alpha = 1)$, three zones are distinguished (see Figure 5). In zone I, the Hopf curve (in the R–a plane) is always supercritical and has no degeneracy. In zone II, the Hopf curve has two

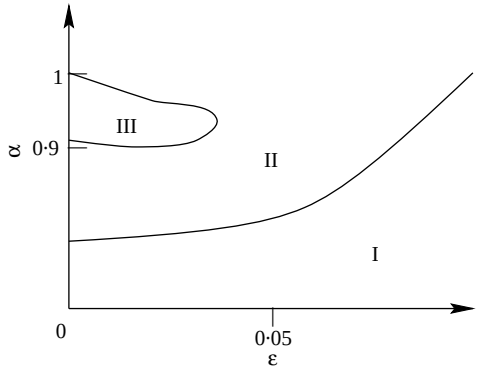

Figure 5. Different zones in the ε–α plane (in the neighbourhood of the point (0, 1)) according to the number of zeroes of a_3: none in zone I, two in zone II and four in zone III.

degeneracies, and finally, in zone III, it has four degeneracies, changing from supercritical to subcritical and *vice versa* as mentioned earlier.

The study of the vanishing of a_3 in the whole ε–α plane, as well as the presence of higher order degeneracies due to the vanishing of the fifth order normal form coefficient of the Hopf bifurcation a_5 are not considered here.

3. NUMERICAL RESULTS

Some numerical study of system (1), that has been performed with AUTO97 [25] and DSTOOL [26], is now presented. It not only corroborates the previous analytical results, but also put in evidence new global results, as the existence of cusp bifurcations of periodic orbits, period-doubling bifurcations and the presence of chaotic attractors.

Four different situations will be presented. In the first one, a bifurcation diagram where three periodic orbits coexist. In the second, a bifurcation set where a cusp of saddle-node bifurcation of periodic orbits appears. In the third case presented, four canard periodic orbits coexist. In the last case, a period-doubling bifurcation is detected and chaotic attractors will emerge as a consequence of a cascade of such bifurcations.

Firstly, the stable periodic orbit that emanates from the supercritical Hopf bifurcation when $R = 4$, $\varepsilon = 0{\cdot}5$, $\alpha = 2$ has been continued. The corresponding bifurcation diagram is shown in Figure (6) (a), where max x (x-co-ordinate of the equilibrium and maximum x of the periodic orbit) versus a is plotted. Increasing the value of a, the unstable equilibrium point becomes stable at a Hopf bifurcation point (labelled H). A stable periodic orbit emerges from such a supercritical Hopf bifurcation. The branch of periodic orbits exhibits two folds. Then, up to three periodic orbits (two are stable and one non-stable) may coexist (labels 1–3). As usual, solid lines mean stability and dashed lines instability. These three periodic orbits appear, for $a = 0{\cdot}9265$, in Figure 6(b).

A second interesting situation occurs for $\varepsilon = 0{\cdot}95, \alpha = 2$, whose corresponding bifurcation set is shown in Figure (7). There are two degenerate Hopf bifurcation points, which split the Hopf bifurcation curve into three portions, denoted by H_1, H_2 and H_3 in the figure. The middle one, H_2, is subcritical and the other two are supercritical. From each of these degenerate points, a saddle-node bifurcation curve (F_1 and F_2, respectively) emanates. Both curves meet at a cusp C. Then, the parameter plane is divided into four regions, labelled (1)–(4), with zero, one, two or three periodic orbits respectively. The configurations of periodic orbits and equilibria in each region is also sketched.

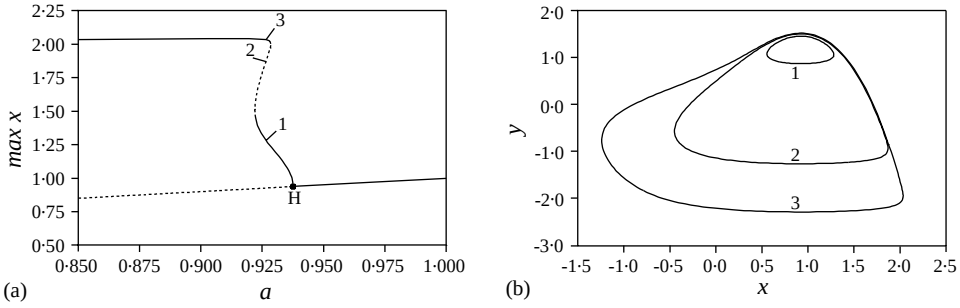

Figure 6. For $R = 4, \varepsilon = 0{\cdot}5, \alpha = 2$: (a) bifurcation diagram max x versus a. Solid line indicates that the equilibrium (or the periodic orbit) is stable whereas dashed line means nonstability. Two saddle-node bifurcations of periodic orbits are present. The equilibrium changes its stability at a Hopf bifurcation, H. (b) Projection onto the x–y plane of the three coexisting periodic orbits for $a = 0{\cdot}9265$.

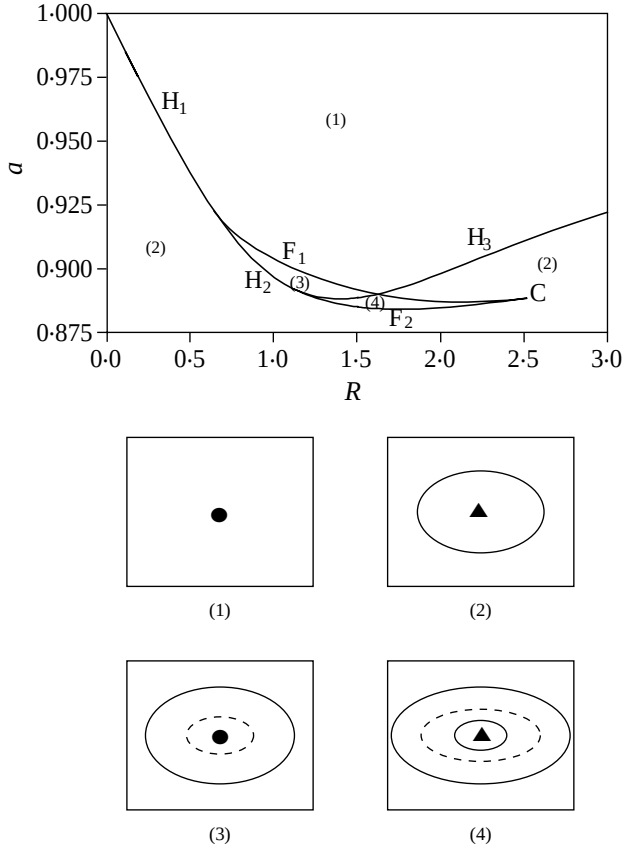

Figure 7. Bifurcation set for $\varepsilon = 0{\cdot}95, \alpha = 2$. The Hopf curve has two supercritical parts (H_1 and H_3) and one subcritical portion (H_2). The fold curves (F_1 and F_2) collapse in a cusp (C). Configurations of equilibria and periodic orbits existing in each zone of the parameter plane are indicated. ●, Stable equilibrium point; ▲, saddle equilibrium point; ———, stable periodic orbit; – – –, saddle periodic orbit.

In the third case, the following values of the parameters are considered: $R = 3$, $\alpha = 0{\cdot}7$ and $\varepsilon = 0{\cdot}001$. The bifurcation diagram period versus a is plotted in Figure 8(a). A zoom of this diagram in the region where canard orbits exist (as a bridge linking the local dynamics,

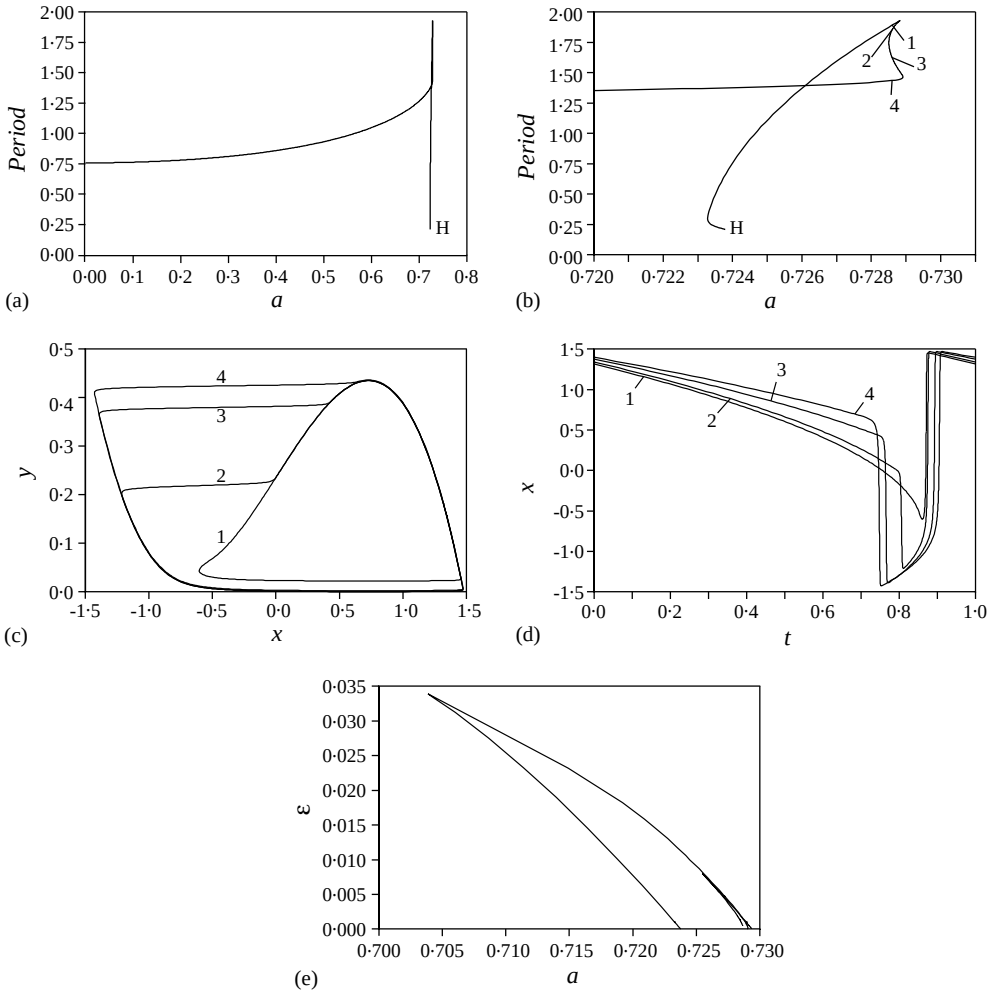

Figure 8. For $R = 3$, $\alpha = 0{\cdot}7$ fixed: (a) bifurcation diagram (period versus a) for $\varepsilon = 0.001$; (b) blow–up of the bifurcation diagram near the Hopf point, H; (c) projection onto the x–y plane of the four coexisting periodic orbits for $a = 0{\cdot}7286$, $\varepsilon = 0{\cdot}001$, labelled in (b); (d) temporal profile (x versus scaled time) of the above-mentioned periodic orbits; (e) loci of folds in the a-ε plane. Note the presence of two cusps (one of them in the bottom right corner).

represented by the small-amplitude limit cycles born in the Hopf bifurcation, and the global dynamics corresponding to relaxation oscillations) appears in Figure 8(b). The branch of periodic orbits that emerge from a Hopf point has up to four saddle-node bifurcations of periodic orbits. Then, four coexisting *canard* orbits are presented for $a = 0{\cdot}7286$ in Figure 8(c). Orbit labelled 1 corresponds to a canard *without head* and the others to canards *with head*. Note that the shape of orbit 4 is very close to a relaxation oscillation. Temporal profiles of these four orbits along a scaled period are shown in Figure 8(d). Different time scales may be observed in such canard periodic orbits. Finally, the continuation of the four folds in the a–ε parameter plane provides the curves drawn in Figure 8(e). Observe the presence of two cusps (one of them in the bottom right corner).

Note that, qualitatively, the bifurcation diagram of Figure 8(a) is similar to the corresponding one in the case of the van der Pol circuit with the battery added as sketched in Figure 1(a). As it is argued in Zvonkin and Shubin [6] (see their Figure 4·7), the period

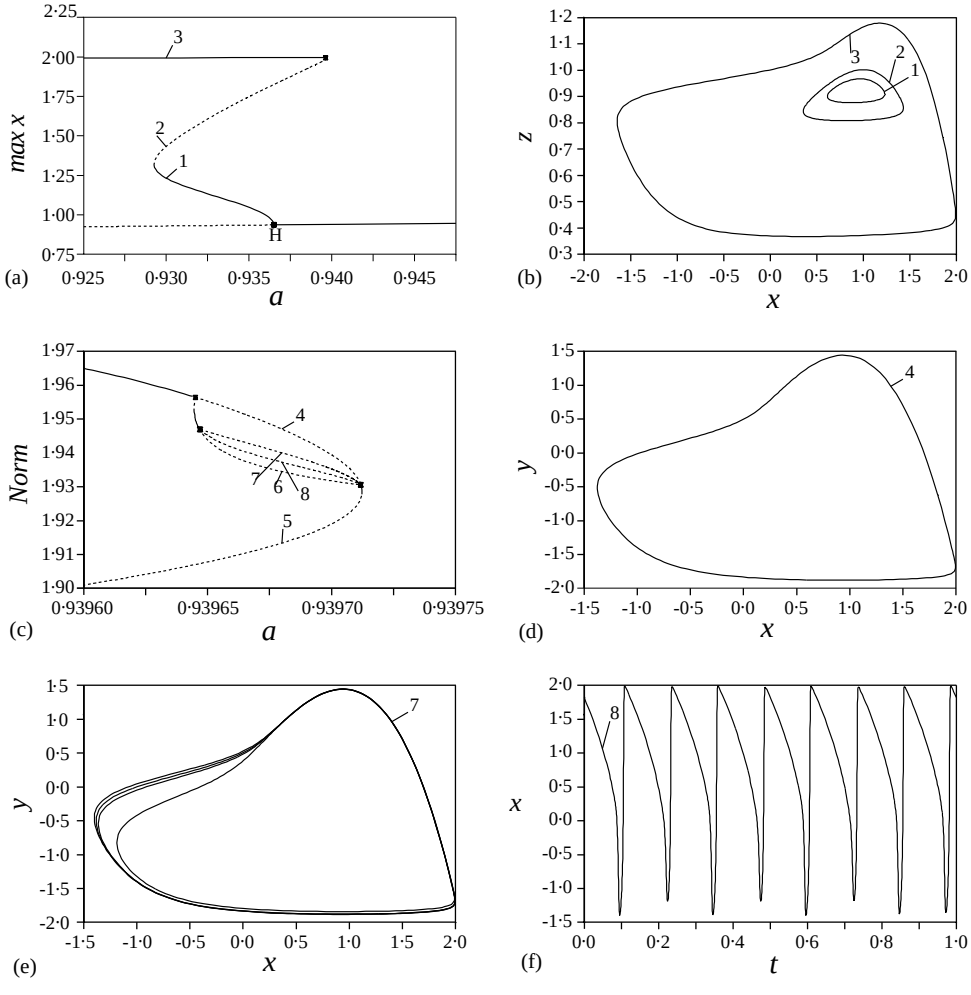

Figure 9. (a) Bifurcation diagram for $R = 4$, $\varepsilon = 0{\cdot}25$, $\alpha = 2$. Solid/dashed curves indicate stable/unstable equilibria or periodic orbits. (b) Three coexisting periodic orbits for $a = 0{\cdot}93$. (c) Blow-up of the bifurcation diagram near the upper fold in (a). (For diagram clarity, the vertical axis is now a scaled L_2-norm.) (d) Projected phase-space representation of orbit 4. (e) Projected phase-space representation of orbit 7 on the second period-doubling branch. (f) Temporal profile (x versus scaled time) of orbit 8 on the third period-doubling branch.

does not simply decrease from the value corresponding to relaxation oscillations but at first increases up to a maximum (for the largest canard without a head) and only then decreases until the Hopf bifurcation (for this reason, on the graph there arises a thin needle). However, the situation in this paper is richer because of the presence of saddle-node bifurcations.

In the last case considered the parameter values fixed are $R = 4$, $\alpha = 2$ and $\varepsilon = 0{\cdot}25$. In Figure 9(a), the bifurcation diagram max x (x-co-ordinate of the equilibrium and maximum x of the periodic orbit) versus a is plotted. Increasing the value of a, the unstable equilibrium point becomes stable at a Hopf bifurcation point (labelled H). A stable periodic orbit emerges from such a supercritical Hopf bifurcation. The branch of periodic orbits exhibits two folds. Then, up to three periodic orbits (two are stable and one non-stable) may coexist (labels 1–3). As in Figure 6(a), solid lines mean stability and dashed lines instability. These three periodic orbits appear, for $a = 0{\cdot}93$, in Figure 9(b). But in this case it is convenient to study more carefully the bifurcation diagram around the upper saddle node of periodic

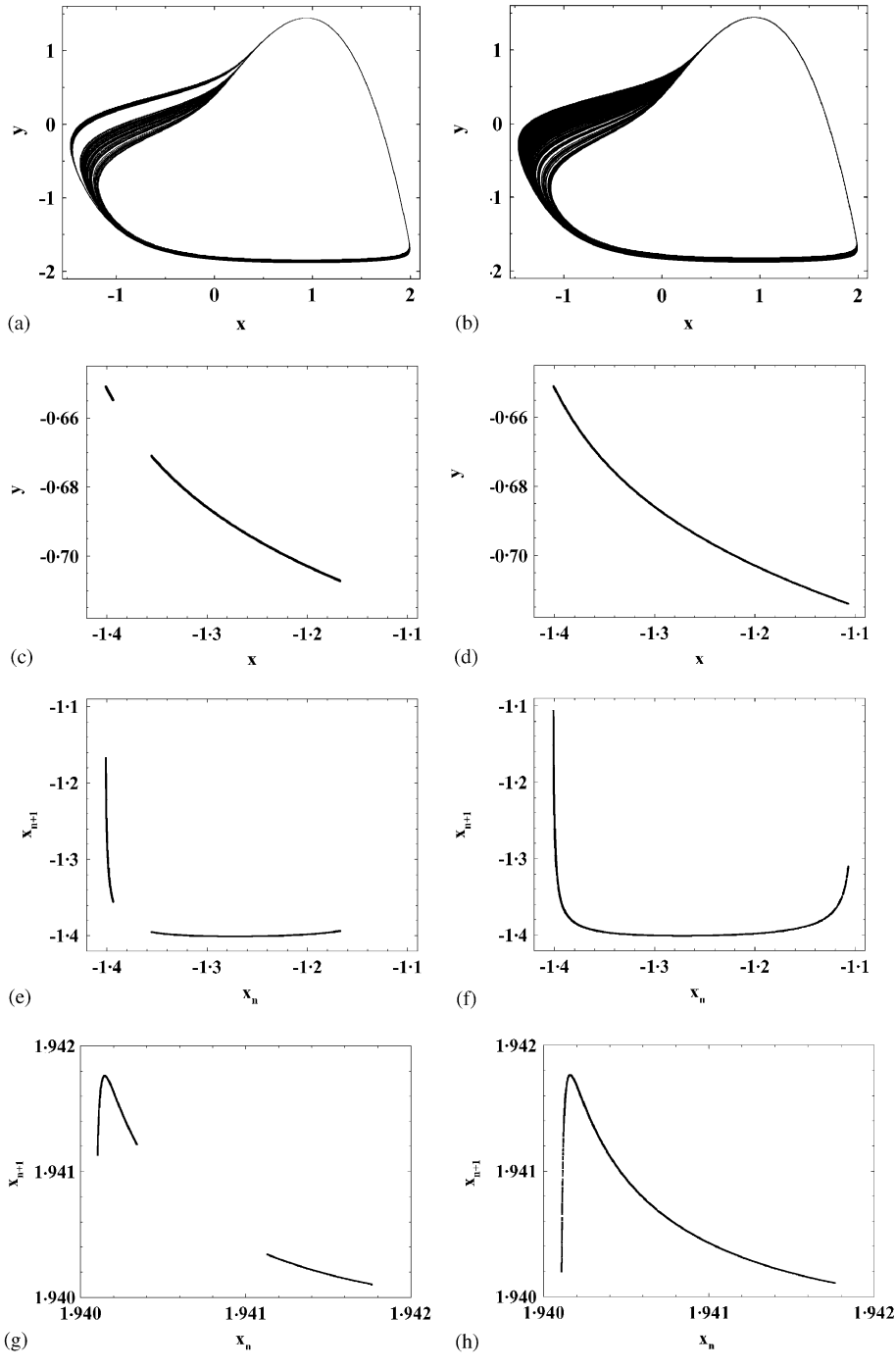

Figure 10. For $R = 4$, $\varepsilon = 0{\cdot}25$, $\alpha = 2$: (a) projected phase-space representation of the chaotic attractor existing for $a = 0{\cdot}939648$; (b) idem for $a = 0{\cdot}9396485$; (c) left intersection of the attractor with the plane $z = 0{\cdot}6$, for $a = 0{\cdot}939648$. (d) idem for $a = 0{\cdot}9396485$; (e) first return map for the left intersection of the attractor with the plane $z = 0{\cdot}6$, for $a = 0{\cdot}939648$; (f) idem for $a = 0{\cdot}9396485$; (g) first return map for the right intersection of the attractor with the plane $z = 0{\cdot}6$, for $a = 0{\cdot}939648$; (h) idem for $a = 0{\cdot}9396485$.

orbits marked with a full black square. The corresponding zoom (for diagram clarity, the vertical axis is now a scaled L_2-norm) is drawn in Figure 9(c), where period-doubling bifurcations are marked with full black squares. A cascade of such period-doubling bifurcations is detected: periodic orbits labelled 4 and 5 stand on the principal branch, orbit 6 is of double period, orbit 7 of period four and orbit 8 is of period eight. Note that the branch of double period has a saddle-node bifurcation on its left part. The projection on the phase space and the temporal profile of some of the labelled orbits appear in Figures 9(d)–9(f).

As the periodic orbits exhibiting the cascade are stable, the existence of a chaotic attractor is expected in that narrow window for parameter a. This chaotic attractor is shown in Figures 10(a)–10(b) for two values of a, respectively, $a = 0{\cdot}939648$ and $0{\cdot}9396485$ (for this last value it is completely developed; compared with periodic orbits shown in Figures 9(d)–9(e)). The use of a section (the plane $z = 0{\cdot}6$) will give information about the structure of such attractor. The corresponding Poincaré map (the left intersection of the attractor with such a plane is shown) appears in Figures 10(c)–10(d). The limit sets of the corresponding Poincaré map for a specific flow section are seemingly unidimensional islands, surely due to their strong contractivity as a consequence of the dissipative character of the system. Whereas two different islands can be observed in Figure 10(c), such islands have joined in Figure 10(d). Now, the first return map corresponding to the Poincaré sections shown above has been represented, respectively, in Figures 10(e)–10(f). A minimum can be observed in both cases. If the first return map is obtained from the right intersection of the attractor with the plane $z = 0{\cdot}6$, a maximum will be present, as can be observed in Figures 10(g)–10(h). This shape reminds the Rössler chaotic attractor of spiral type (see reference [27] and reference [18, Figure 17]. A deeper study of these chaotic attractors is beyond the scope of this paper.

4. CONCLUSIONS

The addition of a new branch to the van der Pol circuit with battery (see Figure 1) gives rise to a three-dimensional system that keeps an important common feature with that: the presence of one equilibrium alone. This fact does not allow the exhibition of other bifurcations but only Hopf.

Recall that other modified van der Pol circuits found in the literature (see references [13–18]) may have more than one equilibrium and then other local bifurcations of equilibria may arise (for example, fold, pitchfork in symmetric systems, Takens–Bogdanov, Hopf–pitchfork and triple–zero). Bifurcation theory guarantees that those systems may exhibit bifurcations of periodic orbits (saddle-node, torus bifurcation, period-doubling and others of higher codimension) and global connections (homoclinic and heteroclinic orbits) that leads to very complicated periodic and quasiperiodic motions (see, for instance, references [18, 28–30] and the references therein).

The system proposed in this paper presents a great richness of folds of periodic orbits as a consequence of degenerations in the Hopf bifurcation. In this way, the analysis of the reduced system has resulted very useful in the understanding of the bifurcation behaviour of the full system for small ε. Moreover, a careful numerical analysis has allowed the detection of a cascade of period-doubling bifurcations and of a chaotic attractor.

The analysis of the modified van der Pol circuit proposed in the present paper should be completed in the future in several ways. On the one hand, the study of the vanishing of the third order normal form coefficient of the Hopf bifurcation a_3 in the whole ε–α parameter plane has to be performed as well as the possibility of higher order degeneracies in the Hopf bifurcation.

On the other hand, a more detailed numerical study of fold and period-doubling bifurcations would determine if other more degenerate bifurcations of periodic orbits may occur (for instance, swallowtail and Takens–Bogdanov). The possible existence of torus bifurcations and of global connections (homoclinic orbits) has also to be elucidated.

With respect to chaotic attractors, more efforts have to be done in order to see their evolution, to understand their structure and to study the possibility of their existence (for small ε) in the canard region.

ACKNOWLEDGMENTS

This work has been partially supported by the *Comisión Interministerial de Ciencia y Tecnología* in the frame of the project PB98-1152 and by the *Consejería de Educación de la Junta de Andalucía* (TIC-0130).

REFERENCES

1. B. VAN DER POL 1927 *London, Edinburgh and Dublin Philosophical Magazine* **3**, 65–80. Forced oscillations in a circuit with nonlinear resistance (receptance with reactive triode).
2. J. GRASMAN 1987 *Asymptotic Methods for Relaxation Oscillations and Applications*. Berlin: Springer-Verlag.
3. J. L. CALLOT, F. DIENER and M. DIENER 1978 *Comptes Rendus des Seances de l'Academie des Sciences. Serie I. Mathematique* **23**, 1059–1061. Le problème de la "Chasse au canard".
4. E. BENOIT, J. L. CALLOT, F. DIENER and M. DIENER 1981 *Collectanea Mathematica* **31–32**, 37–119. Chasse au canard.
5. M. DIENER 1984 *The Mathematical Intelligencer* **6**, 38–49. The canard unchained or how fast/slow dynamical problems bifurcate.
6. A. K. ZVONKIN and M. A. SHUBIN 1984 *Russian Mathematical Surveys* **39**, 69–131. Non-standard analysis and singular perturbations of ordinary differential equations.
7. W. ECKHAUS 1983 in *Asymptotic Analysis* II, Lecture Notes in Mathematics, Vol. 985, 449–494. Berlin: Springer-Verlag. Relaxation oscillations including a standard chase on French ducks.
8. F. DUMORTIER and R. ROUSSARIE 1996 *Canard Cycles and Center Manifolds*, Vol. 121. Memoirs of the American Mathematical Society.
9. E. FREIRE, E. GAMERO and A. J. RODRÍGUEZ–LUIS 1999 *Applied Mathematics Letters* **12**, 73–78. First-order approximation for canard periodic orbits in a van der Pol electronic oscillator.
10. M. KRUPA and P. SZMOLYAN 2001 *Journal of Differential Equations* **174**, 312–368. Relaxation oscillations and canard explosion.
11. P. SZMOLYAN and M. WECHSELBERGER 2001 *Journal of Differential Equations* **177**, 419–453. Canards in $\mathbb{R}^3$.
12. J. GUCKENHEIMER, K. HOFFMAN and W. WECKESSER 2000 *International Journal of Bifurcation and Chaos* **10**, 2669–2687. Numerical computation of canards.
13. R. SHINRIKI, M. YAMAMOTO and S. MORI 1981 *IEEE Proceedings* **69**, 394–395. Multimode oscillations in a modified van der Pol oscillator containing a positive nonlinear conductance.
14. E. FREIRE, L. G. FRANQUELO and J. ARACIL 1984 *IEEE Transactions on Circuits and Systems* **31**, 237–247. Periodicity and chaos in an autonomous electronic system.
15. T. MATSUMOTO, L. O. CHUA and M. KOMURO 1985 *IEEE Transactions on Circuits and Systems* **32**, 797–818. The double scroll.
16. M. G. M. GOMES and G. P. KING 1992 *Physical Review A* **46**, 3100–3110. Bistable chaos II. Bifurcation analysis.
17. J. J. HEALEY, D. S. BROOMHEAD, K. A. CLIFFE, R. JONES and T. MULLIN 1991 *Physica D* **48**, 322–339. The origins of chaos in a modified van der Pol oscillator.
18. E. FREIRE, A. J. RODRÍGUEZ–LUIS, E. GAMERO and E. PONCE 1993 *Physica D* **62**, 230–253. A case study for homoclinic chaos in an autonomous electronic oscillator. A trip from Takens–Bogdanov to Hopf-Shil'nikov.
19. J. GUCKENHEIMER and P. HOLMES 1986 *Nonlinear Oscillations, Dynamical Systems, and Bifurcations of Vector Fields*, Applied Mathematical Sciences, Vol. 42. New York: Springer-Verlag.

20. N. FENICHEL 1983 *SIAM Journal of Mathematical Analysis* **14**, 861–875. Oscillatory bifurcations in singular perturbation theory.
21. B. WEGNER 1989 *Mathematische Nachrichten* **140**, 37–48. About generalized Hopf bifurcation for singularly perturbed systems.
22. E. FREIRE, E. GAMERO and E. PONCE 1989 in *Computers and Mathematics* (E. Kaltofen and S.M. Watt, editors), 109–118. New York: Springer-Verlag. An algorithm for symbolic computation of Hopf bifurcation.
23. Y. A. KUZNETSOV 1998 *Elements of Applied Bifurcation Theory*, Applied Mathematical Sciences Vol. 112, New York: Springer-Verlag.
24. E. FREIRE, E. GAMERO, E. PONCE and L. G. FRANQUELO 1988 in *Symbolic and Algebraic Computations* (P. Gianni, editor) Lecture Notes in Computer Science, Vol. 358, 218–230. Berlin: Springer-Verlag. An algorithm for symbolic computation of center manifolds.
25. E. DOEDEL, A. R. CHAMPNEYS, T. FAIRGRIEVE, Y. A. KUZNETSOV, B. SANDSTEDE and X. WANG 1998 *AUTO*97, *Continuation and Bifurcation Software for Ordinary Differential Equations* (*with HomCont*), Reference Manual, Concordia University.
26. J. GUCKENHEIMER, M. R. MYERS, F. J. WICKLIN and P. A. WORFOLK 1995 *DSTOOL*: *A Dynamical System Toolkit with a Interactive Graphical Interface*, *Reference Manual*, Center for Applied Maths., Cornell University.
27. O. E. RÖSSLER 1979 in *Bifurcation Theory and Applications in Scientific Disciplines* (O. Gurel and O. E. Rössler, editors), Annals of the New York Academy of Sciences, Vol. 316, 376–392. Continuous chaos—four prototype equations.
28. A. ALGABA, E. FREIRE, E. GAMERO and A. J. RODRÍGUEZ–LUIS 1999 *Nonlinearity* **12**, 1177–1206. A three-parameter study of a degenerate case of the Hopf-pitchfork bifurcation.
29. A. ALGABA, E. FREIRE, E. GAMERO, M. MERINO and A. J. RODRÍGUEZ–LUIS 2001 *International Journal of Bifurcation and Chaos*, to appear. Some results on Chua's equation near a triple-zero linear degeneracy.
30. A. ALGABA, F. FERNÁNDEZ–SÁNCHEZ, E. FREIRE, E. GAMERO and A. J. RODRÍGUEZ–LUIS 2002 *Journal of Sound and Vibration* **249**, 899–907 Oscillation–sliding in a modified van der Pol–Duffing electronic oscillator. doi: 10.1006/jsvi.2001.3931